Dynamic Manipulability of the Center of Mass: A Tool to Study, Analyse and Measure Physical Ability of Robots

Dynamic Manipulability of the Center of Mass: A Tool to Study, Analyse and Measure Physical Ability of Robots

Morteza Azad[1], Jan Babič[2] and Michael Mistry[3]

***Abstract*— This paper introduces dynamic manipulability of the center of mass (CoM) as a metric to measure robots' physical abilities to accelerate their CoMs in different directions. By decomposing the effects of velocity dependent constraints, such as unilateral contacts and friction cones, CoM dynamic manipulability is defined as a velocity independent metric which depends only on robot's configuration and inertial parameters. Thus, this metric is independent of any choice of controller and expresses only physical abilities of robots. This important property makes the proposed metric a proper tool to study, analyse and design current and future robots. The outcome of the CoM dynamic manipulability analysis in this paper is an ellipsoid in the CoM acceleration space which graphically shows accessible points due to the unit weighted norm of joint torques. Physical meanings and concepts of two reasonable choices for the weighting matrix, which is used in the weighted norm of joint torques, are discussed and illustrative examples are presented. Since the proposed metric measures physical ability to accelerate the CoM, it is claimed to be a suitable tool to study balance ability of legged robots.**

I. INTRODUCTION

Over the last years, many balance criteria for legged robots have been proposed in order to help to design balancing controllers. Among them, zero moment point (ZMP) [19], [20] or center of pressure (CoP), foot rotation indicator (FRI) [7] and zero rate of change of angular momentum (ZRAM) [8] are most famous and applicable ones. Unfortunately, most of the above mentioned criteria are not well-defined when the robot has multiple non-planar contacts with its environment [8]. The other problem with these criteria is that none of them is able to distinguish between different balanced configurations of a robot in terms of the ability to keep the balance. For example, a legged robot is in balance if the rate of change of its momentum is zero, according to ZRAM, or if its ZMP or CoP is inside the convex hull of the supporting area, according to ZMP and CoP criteria. However, none of these criteria explain the difference between configurations (or robot states) which have the same ZMP, CoP or the rate of change of momentum. In other words, based on the above mentioned criteria, all balanced configurations for a robot are the same as long as they meet the criteria. Here, we tackle this problem and introduce CoM dynamic manipulability as a metric that quantitatively evaluates the physical ability of a robot to accelerate its CoM in different postural and contact configurations. Since the CoM plays a key role in a balancing motion, the ability to accelerate this point can be defined as a robot's ability to balance. Also, the proposed metric is configuration dependent only which enables it to evaluate different configurations in the sense of balance ability.

Unlike the end-effector manipulability, which is a well-developed topic [2], [5], [10], [16], [21], [22], there have not been many studies on CoM manipulability in the literature. Naksuk and Lee [14] introduced ZMP manipulability as an extension to the ZMP balance criterion based on the concept of dynamic manipulability of end-effectors. Then, Cotton *et al.* [3] were the first to introduce dynamic manipulability of the CoM for humanoid robots. They used dynamic motion equations to calculate the CoM acceleration due to available joint torques. The result was a polyhedron in the CoM acceleration space and also a sphere inside the polyhedron as an approximation to that space. Recently, Gu *et al.* [9] proposed feasible CoM dynamic manipulability (FCDM) for planar humanoids. To evaluate the feasibility of the manipulability index, they considered the ground-contact force constraints such as friction cone and unilaterlaity of the normal force for single support phase of a planar humanoid. However, their proposed method is not developed for floating base robots with multiple contacts and also it is dependent on the robot's joint velocities (i.e. a velocity dependent index). Featherstone [6] was the first to introduce a metric to evaluate physical ability of a robot to balance on a single point. By using impulsive dynamics, this metric was defined as the ratio between instantaneous change of the CoM velocity and instantaneous changes of joint accelerations, due to impulses at the actuated joints.

In this paper, we calculate CoM dynamic manipulability by using motion equations of floating base robots which have multiple contacts with the environment. Thus, in our manipulability analysis, we take into account the effects of inertial parameters as well as under-actuation and kinematics constraints. The under-actuation is due to the floating base and kinematic constraints are due to multiple contacts with the environment, such as hands and feet for biped robots. As a result of the manipulability analysis, we obtain an ellipsoid which graphically shows the CoM acceleration due to the weighted unit norm of torques at the actuated joints. The weights should be set by the user and based on the application. Two physically meaningful choices for the weights are introduced in this paper and their concepts are discussed. The proposed CoM dynamic manipulability is a configuration based (i.e. velocity independent) metric which is dependent only on the physical properties of a robot and its configuration and it is applicable to all types of legged

[1]School of Computer Science, University of Birmingham, Edgbaston, The United Kingdom

[2]Department of Automation, Biocybernetics and Robotics, Jožef Stefan Institute, Jamova cesta 39, SI-1000, Ljubljana, Slovenia

[3]School of Informatics, University of Edinburgh, The United Kingdom contact email: m.azad at bham.ac.uk

(floating base) robots with different contact conditions. Also, since this metric studies the motion of the CoM, it provides a proper tool to study balancing abilities of robots and design new robots with higher physical abilities to balance.

II. Dynamic Manipulability of the CoM

The concept of manipulability (of end-effectors) for manipulators, first introduced by Yoshikawa [21]. He proposed that $\sqrt{\mathbf{J}_e\mathbf{J}_e^T}$, where $\mathbf{J}_e$ is the Jacobian of end-effector, can be used to measure the capability of a manipulator in a specific configuration. He also extended this metric to dynamic manipulability by including the dynamics equations of manipulators [22]. However, Doty *et. al.* [5] pointed out that $\sqrt{\mathbf{J}_e\mathbf{J}_e^T}$ has no physical meaning when dealing with general robots with a combination of different joint types (e.g. revolute and prismatic joints). They proposed to use a weighting matrix to solve this issue and make consistency in the units.

In this section, we calculate dynamic manipulability ellipsoid of the CoM which shows the effects of unit weighted joint torques on the CoM accelerations. Let $\mathbf{q} \in \mathbb{R}^n$ denote the vector of generalized coordinates of a floating-base robot which has 6 virtual unactuated degrees of freedom (DoF) due to its floating base. Assume that there are l linearly independent kinematic constraints acting on the robot. These constraints are either due to the kinematic loops in the mechanism or contacts with the environment. The latter models the hands and feet contacts for a humanoid or a legged robot. The motion equations of this robot will be

$$\mathbf{M}(\mathbf{q})\ddot{\mathbf{q}} + \mathbf{h}(\mathbf{q},\dot{\mathbf{q}}) + \mathbf{g}(\mathbf{q}) = \mathbf{B}\boldsymbol{\tau} + \mathbf{J}_c^T(\mathbf{q})\,\mathbf{f}_c\,, \qquad (1)$$

where $\mathbf{M} \in \mathbb{R}^{n\times n}$ is the joint-space inertia matrix, $\mathbf{h} \in \mathbb{R}^n$ is the vector of centripetal and Coriolis forces, $\mathbf{g} \in \mathbb{R}^n$ is the vector of gravity force, $\mathbf{B} \in \mathbb{R}^{n\times k}$ is the selection matrix for the actuated joints, $\boldsymbol{\tau} \in \mathbb{R}^k$ is the vector of actuated joint torques, $\mathbf{J}_c \in \mathbb{R}^{l\times n}$ is the Jacobian of the constraints and $\mathbf{f}_c \in \mathbb{R}^l$ is the vector of the constraint forces.

Assuming that there is no sliding or loss of contact (i.e. kinematic constraints are bilateral), we will have

$$\mathbf{J}_c\dot{\mathbf{q}} = \mathbf{0} \implies \dot{\mathbf{J}}_c\dot{\mathbf{q}} + \mathbf{J}_c\ddot{\mathbf{q}} = \mathbf{0}\,. \qquad (2)$$

By multiplying both sides of (1) by $\mathbf{J}_c\mathbf{M}^{-1}$ and employing (2), we obtain

$$\mathbf{f}_c = -(\mathbf{J}_c\mathbf{M}^{-1}\mathbf{J}_c^T)^{-1}[\dot{\mathbf{J}}_c\dot{\mathbf{q}} + \mathbf{J}_c\mathbf{M}^{-1}(\mathbf{B}\boldsymbol{\tau} - \mathbf{h} - \mathbf{g})]\,. \quad (3)$$

Substituting $\mathbf{f}_c$ from (3) into (1) and solving for $\ddot{\mathbf{q}}$, yields

$$\ddot{\mathbf{q}} = \mathbf{J}_q\boldsymbol{\tau} + \ddot{\mathbf{q}}_{vg}\,, \qquad (4)$$

where

$$\mathbf{J}_q = \mathbf{P}_M\mathbf{M}^{-1}\mathbf{B}\,, \qquad (5)$$

and $\ddot{\mathbf{q}}_{vg}$ is a part of the joint accelerations due to the gravity and joint velocities as

$$\ddot{\mathbf{q}}_{vg} = -\mathbf{P}_M\mathbf{M}^{-1}(\mathbf{h}+\mathbf{g}) - \mathbf{J}_{c_M}^{\#}\dot{\mathbf{J}}_c\dot{\mathbf{q}}\,, \qquad (6)$$

and

$$\mathbf{P}_M = \mathbf{I} - \mathbf{J}_{c_M}^{\#}\mathbf{J}_c\,, \qquad (7)$$

where $\mathbf{I} \in \mathbb{R}^{n\times n}$ is an identity matrix and

$$\mathbf{J}_{c_M}^{\#} = \mathbf{M}^{-1}\mathbf{J}_c^T(\mathbf{J}_c\mathbf{M}^{-1}\mathbf{J}_c^T)^{-1}\,, \qquad (8)$$

is a generalized inverse of $\mathbf{J}_c$ with the joint-space inertia matrix as the weighting matrix [4].

Let $\mathbf{c} \in \mathbb{R}^3$ and $\mathbf{J} \in \mathbb{R}^{3\times n}$ denote the position and Jacobian of the CoM in the world frame, respectively. Note that, Jacobian of the CoM is a well-studied subject in the literature [1], [11], [12], [13], [15], [17], [18]. Then, the velocity of the CoM will be $\dot{\mathbf{c}} = \mathbf{J}\dot{\mathbf{q}}$ and therefore, the CoM acceleration is

$$\ddot{\mathbf{c}} = \dot{\mathbf{J}}\dot{\mathbf{q}} + \mathbf{J}\ddot{\mathbf{q}} = \mathbf{J}_\tau\boldsymbol{\tau} + \ddot{\mathbf{c}}_{vg}\,, \qquad (9)$$

where

$$\mathbf{J}_\tau = \mathbf{J}\mathbf{P}_M\mathbf{M}^{-1}\mathbf{B}\,, \qquad (10)$$

and $\ddot{\mathbf{c}}_{vg}$ is the gravity and velocity dependent part of the CoM acceleration which is

$$\ddot{\mathbf{c}}_{vg} = \mathbf{J}\ddot{\mathbf{q}}_{vg} + \dot{\mathbf{J}}\dot{\mathbf{q}}\,. \qquad (11)$$

Matrix $\mathbf{J}_\tau$ can be regarded as a Jacobian that maps the joint torques to the CoM acceleration. Note that $\mathbf{J}_\tau$ is independent of the robot's velocity whereas $\ddot{\mathbf{c}}_{vg}$ is dependent on both configuration and velocity of the robot. Here, we assume that there is no constraint on the movement of the CoM and therefore $\mathbf{J}_\tau$ is full row rank. In case that the CoM has only 2 DoF (i.e. constrained motion of the CoM), we introduce a new frame oriented such that its x and y axes span the space of motion freedoms of the CoM, and redefine $\ddot{\mathbf{c}}$ to be a 2D vector. Likewise, if the CoM has only one DoF then we introduce a new frame with its x axis in the direction of motion freedom, and define $\ddot{\mathbf{c}}$ to be a 1D vector. Hence, the Jacobian in the new frame will be full row rank but it will have a lower dimension than $\mathbf{J}_\tau$. The above explanation is for the sake of mathematical soundness, though there might not be any practical example of a robot with a constrained motion of its CoM.

The unit weighted norm of actuated joint torques can be defined as

$$\boldsymbol{\tau}^T\mathbf{W}_\tau\boldsymbol{\tau} = 1\,, \qquad (12)$$

where $\mathbf{W}_\tau$ is a weighting matrix and assumed to be symmetric and positive definite. The reason of using $\mathbf{W}_\tau$ is to unify the units and strengths of different actuated joints. By inverting (9), we can write

$$\boldsymbol{\tau} = \mathbf{J}_\tau^{\#}(\ddot{\mathbf{c}} - \ddot{\mathbf{c}}_{vg}) + \mathbf{N}_\tau\,\boldsymbol{\tau}_0\,, \qquad (13)$$

where $\mathbf{N}_\tau = \mathbf{I} - \mathbf{J}_\tau^{\#}\mathbf{J}_\tau$ is the projection matrix to the null-space of $\mathbf{J}_\tau$, and

$$\mathbf{J}_\tau^{\#} = \mathbf{W}_\tau^{-1}\mathbf{J}_\tau^T(\mathbf{J}_\tau\mathbf{W}_\tau^{-1}\mathbf{J}_\tau^T)^{-1}\,, \qquad (14)$$

is a generalized inverse of $\mathbf{J}_\tau$. Thus, by replacing (13) into (12), we will have

$$\begin{aligned} 1 \;=\; & (\mathbf{J}_\tau^{\#}(\ddot{\mathbf{c}} - \ddot{\mathbf{c}}_{vg}) + \mathbf{N}_\tau\boldsymbol{\tau}_0)^T\mathbf{W}_\tau(\mathbf{J}_\tau^{\#}(\ddot{\mathbf{c}} - \ddot{\mathbf{c}}_{vg}) + \mathbf{N}_\tau\,\boldsymbol{\tau}_0) \\ =\; & (\ddot{\mathbf{c}} - \ddot{\mathbf{c}}_{vg})^T\mathbf{J}_\tau^{\#T}\mathbf{W}_\tau\mathbf{J}_\tau^{\#}(\ddot{\mathbf{c}} - \ddot{\mathbf{c}}_{vg}) \\ & + (\ddot{\mathbf{c}} - \ddot{\mathbf{c}}_{vg})^T(\mathbf{J}_\tau^{\#T}\mathbf{W}_\tau\mathbf{N}_\tau)\boldsymbol{\tau}_0 \\ & + \boldsymbol{\tau}_0^T(\mathbf{N}_\tau^T\mathbf{W}_\tau\mathbf{J}_\tau^{\#})(\ddot{\mathbf{c}} - \ddot{\mathbf{c}}_{vg}) + \boldsymbol{\tau}_0^T\mathbf{N}_\tau^T\mathbf{W}_\tau\mathbf{N}_\tau\boldsymbol{\tau}_0\,. \end{aligned}$$

Note that, according to definitions of $\mathbf{J}_\tau^\#$ and $\mathbf{N}_\tau$, we have $\mathbf{J}_\tau^{\#T}\mathbf{W}_\tau\mathbf{N}_\tau = \mathbf{N}_\tau^T\mathbf{W}_\tau\mathbf{J}_\tau^\# = 0$. Hence,

$$1 = (\ddot{\mathbf{c}} - \ddot{\mathbf{c}}_{vg})^T\mathbf{J}_\tau^{\#T}\mathbf{W}_\tau\mathbf{J}_\tau^\#(\ddot{\mathbf{c}} - \ddot{\mathbf{c}}_{vg}) + \boldsymbol{\tau}_0^T\mathbf{N}_\tau^T\mathbf{W}_\tau\mathbf{N}_\tau\boldsymbol{\tau}_0\,.$$

Since $\mathbf{W}_\tau$ is positive definite, both terms in the right hand side of the above equation are positive. Thus, removing the last term yields an inequality as

$$0 \leq (\ddot{\mathbf{c}} - \ddot{\mathbf{c}}_{vg})^T\mathbf{J}_\tau^{\#T}\mathbf{W}_\tau\mathbf{J}_\tau^\#\,(\ddot{\mathbf{c}} - \ddot{\mathbf{c}}_{vg}) \leq 1 \qquad (15)$$

and therefore, by employing (14), we will have

$$0 \leq (\ddot{\mathbf{c}} - \ddot{\mathbf{c}}_{vg})^T(\mathbf{J}_\tau\mathbf{W}_\tau^{-1}\mathbf{J}_\tau^T)^{-1}(\ddot{\mathbf{c}} - \ddot{\mathbf{c}}_{vg}) \leq 1\,. \qquad (16)$$

The above inequality defines an ellipsoid in the acceleration space which represents the acceleration of the CoM due to the unit weighted norm of torques at the actuated joints. The center of this ellipsoid is $\ddot{\mathbf{c}}_{vg}$ and its radii and orientation can be determined by the eigenvectors and eigenvalues of matrix $\mathbf{J}_\tau\mathbf{W}_\tau^{-1}\mathbf{J}_\tau^T$. Therefore, the size and shape of the ellipsoid is configuration dependent only. Velocity and gravity only alter the location of the ellipsoid within the space of the CoM acceleration. Note that, according to (16), this ellipsoid captures the effect of both under-actuation (due to the floating base) and kinematic constraints (due to the contacts) in the relationship between the CoM acceleration and torques at the actuated joints.

Note that, the analysis presented in this section is applicable to planar robots, in which case $n = k + 3$, $\ddot{\mathbf{c}} \in \mathbb{R}^2$ and the ellipsoid becomes ellipse.

III. Discussion on Concept and Application

As previously mentioned in this paper, dynamic manipulability of the CoM is a metric that can be used to measure the physical ability of a mechanism to accelerate its CoM. It graphically shows the acceleration of the CoM in different directions which can be used to analyse existing robots and also designing new robots in terms of CoM manipulability. According to (16), shape and size of the ellipsoid are dependent on the robot's configuration, its inertial parameters, kinematic constraints and also the weighting matrix. Among these factors, weighting matrix is the only one that has to be chosen by the user and based on the application. Note that, defining proper $\mathbf{W}_\tau$ is quite important since it significantly affects the size and shape of the ellipsoid. None of the previous studies on manipulability, including the well-developed area of end-effector manipulability, has studied the effects of the weighting matrix nor discussed possible meaningful choices for this matrix.

In this section, we introduce two reasonable choices for $\mathbf{W}_\tau$ and discuss their physical meanings and their applications in studying and measuring robot's physical ability to manipulate its CoM. The suggested choices are defined in a general way so they can also be used for end-effector dynamic manipulability analysis. Note that, the application of the CoM dynamic manipulability proposed in this paper is not limited to the suggested options for $\mathbf{W}_\tau$ and users can define their weighting matrices to suit their applications. For example, an identity matrix can be chosen when all joints are the same type and able to generate same amount of torque (or the user cares about generating torques at all joints equally).

A. First Choice: Torque Limits

One first proposed reasonable choice for $\mathbf{W}_\tau$ is

$$\mathbf{W}_\tau^{-1} = \text{diag}([k\boldsymbol{\tau}_{1_{max}}^2, k\boldsymbol{\tau}_{2_{max}}^2, \ldots, k\boldsymbol{\tau}_{k_{max}}^2])\,, \qquad (17)$$

where $\boldsymbol{\tau}_{i_{max}}$ is the saturation limit at the ith joint ($i = 1, 2, ..., k$) and $|\boldsymbol{\tau}_i| \leq \boldsymbol{\tau}_{i_{max}}$. By using this weighting matrix, (12) will become

$$\frac{\boldsymbol{\tau}_1^2}{\boldsymbol{\tau}_{1_{max}}^2} + \frac{\boldsymbol{\tau}_2^2}{\boldsymbol{\tau}_{2_{max}}^2} + \cdots + \frac{\boldsymbol{\tau}_k^2}{\boldsymbol{\tau}_{k_{max}}^2} = k\,. \qquad (18)$$

Since the ellipsoid in (18) accommodates all combinations of available joint torques (i.e. $\boldsymbol{\tau}_i^2/\boldsymbol{\tau}_{i_{max}}^2 \leq 1$), the outcome ellipsoid in (16) will include all achievable accelerations of the CoM. Observe that, as proved in Section II, all points inside the ellipsoid in (18) map into the ellipsoid in (16).

It is worth mentioning that, the weighting matrix in (17) is different from the one used in [9] to approximate feasible CoM accelerations due to torque limits. The difference is that Gu *et al.* [9] did not include the number of actuators (i.e. k) in their weighting matrix. Removing k from (17), which is the same as replacing k with 1 in the right hand side of (18), results in the unit norm of normalized joint torques based on torque limits as it is mentioned in [9]. It is clear that the outcome ellipsoid, by using their choice of $\mathbf{W}_\tau$, will not include all feasible CoM accelerations and cannot be a reasonable approximation of achievable CoM accelerations due to torque limits.

In order to verify our choice of $\mathbf{W}_\tau$ and to illustrate the relationship between manipulability ellipsoid (ellipse in 2D) by using (17) and achievable CoM accelerations due to torque limits, we plot ellipses for four different planar robots at zero velocity and gravity (i.e. $\ddot{\mathbf{c}}_{vg} = 0$), assuming arbitrary torque limits. These four robots consist of (i) four, (ii) five, (iii) seven and (iv) ten links which are connected to each other by active revolute joints. The first link of each robot is fixed to the ground by a passive revolute joint. Each link is assumed to have unit mass and length and its CoM in the middle. Corresponding robots configurations, which are chosen randomly, are depicted in the top right corner of each plot. Areas of feasible CoM accelerations (due to saturation limits) for these robots are indicated in Fig. 1 by grey and black polygons. These polygons are obtained numerically by mapping points inside the range of available joint torques ($|\boldsymbol{\tau}_i| \leq \boldsymbol{\tau}_{i_{max}}$) to the CoM acceleration space. This mapping is done by using (9). Both polygons for each robot are for a same configuration. The difference is that the black one shows the achievable area when the end point of the last link is fixed (i.e. an extra bilateral constraint). This is to show the effect of an additional constraint on feasible CoM accelerations (and also on ellipses). The extra constraint deforms the feasible area due to (i) the additional kinematic constraint limiting the movements of the CoM in some directions, and (ii) contact forces provide additional torques in some directions. Corresponding manipulability

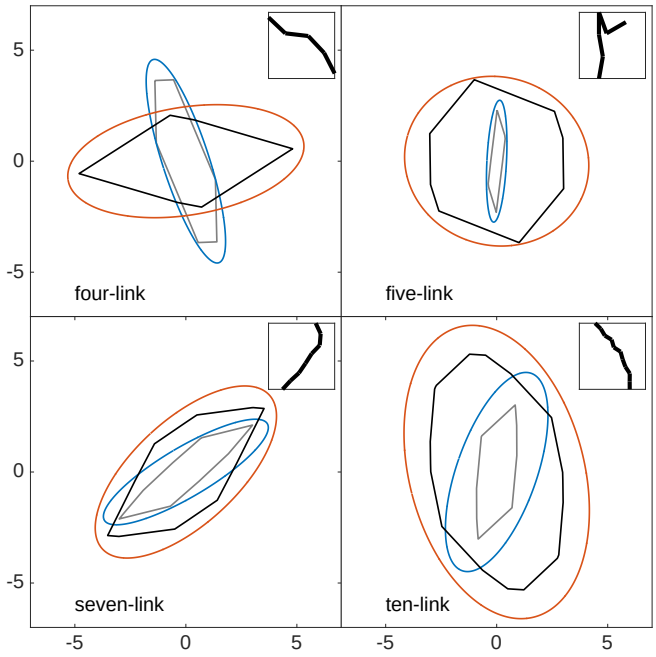

Fig. 1. Feasible CoM acceleration polygons due to torque limits and CoM dynamic manipulability ellipses for four different planar robots. The black polygons and red ellipses are for constrained end-effectors whereas the grey polygons and blue ellipses are for unconstrained robots at the same configuration. The gravity and velocity are assumed to be zero ($\ddot{\mathbf{c}}_{vg} = 0$).

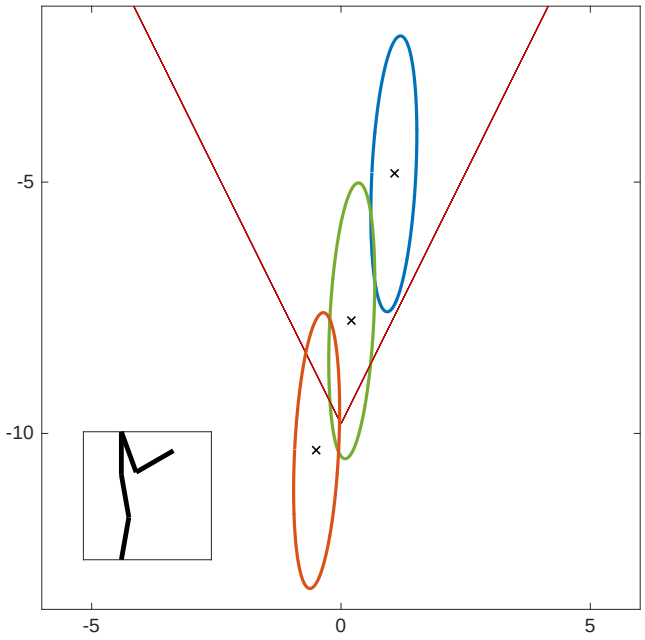

Fig. 2. CoM dynamic manipulability ellipses for a five-link planar robot in different velocities. The robot's configuration is shown on the bottom left corner. Straight lines show the friction cone of the contact force.

ellipses, which are calculated by using the weighting matrix in (17), are also shown in Fig. 1. Red and blue ellipses are related to constrained and unconstrained last links, respectively. Comparing the ellipses and polygons, it can be seen that, by employing (17) as a weighting matrix, these ellipses can provide reasonable approximations of achievable CoM accelerations. It is obvious that calculating ellipses is computationally much more efficient rather than obtaining polygons. Ellipses also provide analytical metrics which can be used to study and optimize a robot's physical ability to manipulate its CoM.

Including gravity and velocity to the above examples will only change center points of the polygons and ellipses and will have no effect on shapes and sizes of those areas. As an example, we consider the five-link robot in the same configuration and same torque limits as we had for the ellipses in the top right corner of Fig. 1. The robot's configuration is shown in the bottom left corner of Fig. 2. The blue ellipse in this figure is the CoM manipulability ellipse for this robot when the gravity exists and velocity is zero. Therefore, the difference between this ellipse and the blue one in the top right corner of Fig. 1 is due to the gravity which only moves the center point ($\ddot{\mathbf{c}}_{vg} \neq 0$). The red and green ellipses in Fig. 2 are also for the same robot and same configuration but different velocities. This implies a kind of decoupling between the effects of inertial parameters and configuration (size and shape of the ellipse) on one hand and velocity (location of the ellipse) on the other hand. This decoupling is important in studying physical ability of a robot in different configurations independent of its velocity.

The inequality (16) for the CoM dynamic manipulability ellipsoid in Section II is derived assuming that the contacts are bilateral. Although in legged robots the contacts are usually unilateral, it is desired to maintain the contacts (except contact switching) and prevent sliding or loss of contact during the robot's performance. Therefore, bilateral contact assumption still makes sense if the contact forces satisfy the unilateral contact constraints. In the example in Fig. 2, replacing the bilateral constraint by a unilateral one in the first link, we can draw friction cone constraints in the CoM acceleration space. Straight lines in Fig. 2 show the CoM acceleration limits due to the friction cone when the coefficient of friction is 0.5. As can be seen in this figure, different velocities result in different feasible areas for a same manipulability ellipse due to the unilateral constraint. It implies that, although the CoM dynamic manipulability ellipse, which is an approximation of the robot's physical ability to accelerate its CoM, remains the same, enabling the robot to exploit that ability is dependent on velocity, as well. Note that, a proper velocity has to be determined by a controller (or a motion planner) in order to exploit available ability of a robot to reach a certain acceleration of the CoM and satisfy the contact conditions.

In the examples in Fig. 2, we assumed a unilateral constraint at the first link of the robot which is the same situation that arises in single support phase for legged robots. Since we also assumed that the first joint is unactuated, the CoP (and also the ZMP) is always at the contact point no matter if the robot is in balance or not. This clarifies the difference between the CoP (or the ZMP) and manipulability ellipses. As can be seen in Fig. 2, ellipses provide information about

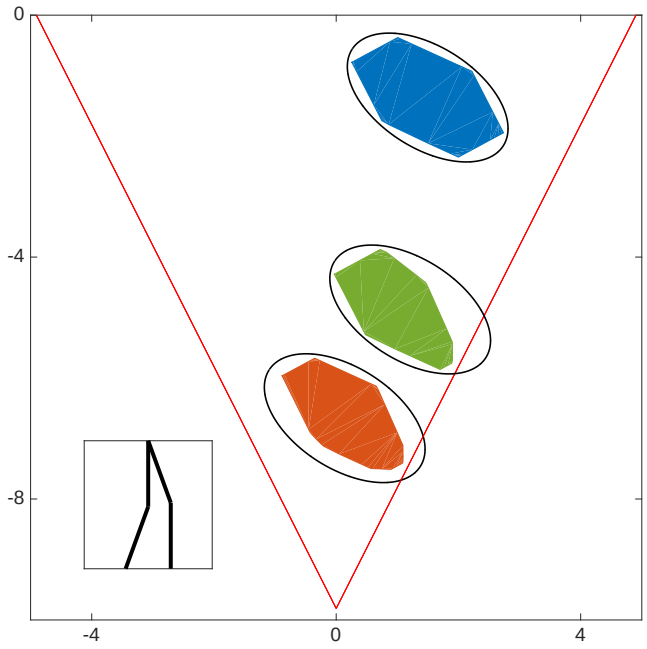

Fig. 3. CoM dynamic manipulability ellipses and feasible CoM acceleration polygons due to torque limits and unilateral constraints of a four-link robot with two contact points in different velocities. Straight lines show the friction cone of the total force.

the robot's ability to accelerate the CoM in different directions with different configurations and velocities, whereas the CoP (or the ZMP) remains at the same point regardless of the robot's states.

It is worth mentioning that a larger ellipse means not only higher physical ability to accelerate the CoM, but also larger feasible region for $\ddot{\mathbf{c}}_{vg}$ to include a desired point in the CoM acceleration space inside the ellipse. In other words, although the ellipse's position and therefore its feasible part due to the unilateral constraint is dependent on $\ddot{\mathbf{c}}_{vg}$, having a larger ellipse provides more options for the controller (or the planner) to choose a proper velocity to reach a desired CoM acceleration.

Introducing more unilateral constraints to the robot (e.g. double support phase in legged robots), or having multiple contacts which at least one of them is unilateral, will result in velocity dependent limits for the CoM acceleration. In this case, each contact has its own friction cone limits which are dependent on robot's states. This is due to the relationship between contact forces and robot's velocity which is stated in (3). Fig. 3 shows manipulability ellipses and their corresponding feasible CoM acceleration areas of a four-link robot in three different velocities. The polygons are obtained numerically and by using (9). The robot's configuration is depicted in the bottom left corner of the graph and it is chosen to mimic double support phase of a planar biped. The blue (top) area shows the feasible area when the velocity is zero and the two others are for randomly chosen velocities. By comparing the three areas, it is obvious that different limits are affecting feasible areas at different velocities which shows the dependency of the limits on the robot's velocity.

As can be seen in Fig. 3, manipulability ellipses are the same for all velocities implying that the robot's physical ability to accelerate its CoM does not depend on velocity. However, the robot's velocity affects the feasibility of the areas due to the unilateral contacts. In other words, in all three velocities, the robot's physical ability to accelerate its CoM is the same, although in two of the velocities (i.e. green and red areas) the robot may lose its contact with the ground if it wants to reach certain accelerations. Therefore, exploiting robot's ability in a certain configuration depends on choosing proper velocity by the controller (or planner), as well. Note that, straight lines in Fig. 3 show the friction cone limits for the total contact force which do not have any effect on feasible areas at the chosen velocities since the areas are already limited by friction cone constraints of individual contact forces.

B. Second Choice: Joint Accelerations

Other than joint torques, joint accelerations are also important factors in studying a robot's physical ability. Obviously, producing less accelerations at the joints, with same amount of joint torques and same CoM acceleration, is desirable since it leads to lower joint velocities and consequently less joint movements. Less movements at the joints is beneficial since the robot's workspace is limited. Also lower joint velocities with same joint torques means less work and higher energy efficiency. Therefore, we introduce a proper weighting matrix in order to study the robot's CoM acceleration due to the limited joint accelerations.

Let $\mathbf{W}_q \in \mathbb{R}^{n\times n}$ denote a symmetric positive definite matrix. We define the second choice of $\mathbf{W}_\tau$ as

$$\mathbf{W}_\tau = \mathbf{J}_q^T \mathbf{W}_q \mathbf{J}_q \,. \tag{19}$$

By substituting (19) into (12), we will have

$$\boldsymbol{\tau}^T \mathbf{W}_\tau \boldsymbol{\tau} = 1 = \boldsymbol{\tau}^T \mathbf{J}_q^T \mathbf{W}_q \, \mathbf{J}_q \boldsymbol{\tau} \,. \tag{20}$$

By employing (4), the above equation becomes

$$(\ddot{\mathbf{q}} - \ddot{\mathbf{q}}_{vg})^T \mathbf{W}_q \, (\ddot{\mathbf{q}} - \ddot{\mathbf{q}}_{vg}) = 1 \,, \tag{21}$$

where $\mathbf{W}_q$ can be used to unify the units or express the relative importance of the joint accelerations in $\ddot{\mathbf{q}}$. The above equation specifies a n-dimensional ellipsoid in the joint acceleration space which its center point is at $\ddot{\mathbf{q}}_{vg}$. This point is the same center point of a n-dimensional ellipsoid that will be obtained if we project the unit weighted norm of joint torques (i.e. Eq. (12)) to the joint acceleration space. Such ellipsoid will be the same as (16) if we replace $\mathbf{J}_\tau$ with $\mathbf{J}_q$ and $\ddot{\mathbf{c}}$ with $\ddot{\mathbf{q}}$.

By choosing $\mathbf{W}_\tau$ as in (19), CoM dynamic manipulability ellipsoid will show an area in the CoM acceleration space which is achievable via unit weighted norm of joint accelerations in (21). Therefore, by setting proper values for $\mathbf{W}_q$ (user's choice based on the application), a user can study the effect of joint accelerations on reaching desired CoM accelerations. As an illustrative example, Fig. 4 shows CoM manipulability ellipses for a five-link planar robot (i.e. the same robot explained earlier in this section) in two different

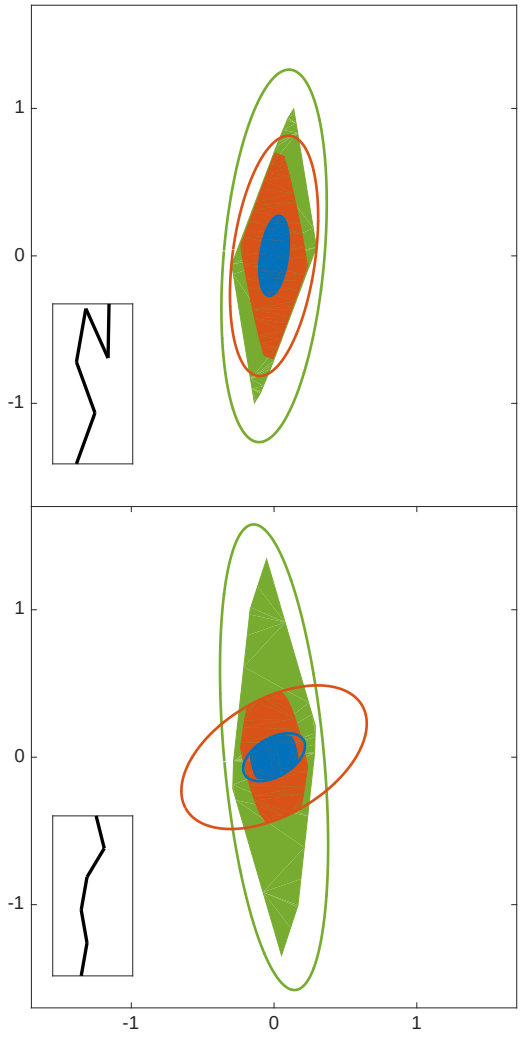

Fig. 4. CoM dynamic manipulability ellipses with different weighting matrices for a planar five-link robot in two configurations. Green areas show feasible CoM accelerations due to torque limits. Blue and red areas show achievable CoM accelerations with unit weighted norms of joint accelerations.

configurations which are shown in bottom left corners of the plots. Without losing generality, we set the gravity and velocity to zero in these examples (i.e. $\ddot{\mathbf{q}}_{vg} = \ddot{\mathbf{c}}_{vg} = 0$). Torque limits for all four actuated joints are assumed to be one. Green areas show feasible CoM accelerations due to the torque limits and green ellipses are their approximations which are obtained by using (17). Blue and red areas indicate CoM accelerations which are achievable by limited norm of the joint accelerations. For the blue areas the norm is one (i.e. $\ddot{\mathbf{q}}^T\ddot{\mathbf{q}} = 1$) and for the red ones the norm is 3 (i.e. $\ddot{\mathbf{q}}^T\ddot{\mathbf{q}} = 9$). Blue and red ellipses are obtained by using (19) and setting $\mathbf{W}_q$ to identity and $1/9$ times identity matrices, respectively, to match the corresponding areas. Green, blue and red areas are obtained numerically and by using (9). In obtaining red and blue areas corresponding joint acceleration limits (i.e. $\ddot{\mathbf{q}}^T\ddot{\mathbf{q}} \leq 1$ for red areas and $\ddot{\mathbf{q}}^T\ddot{\mathbf{q}} \leq 9$ for blue areas) are also considered via (4).

As it is expected, and also can be seen in Fig. 4, blue and red ellipses include all points in the blue and red areas, respectively. Although they also include points which are not inside their corresponding areas. The reason is that the mapping from the joint acceleration space to the CoM acceleration space is not one-to-one, which means that the mapping from the CoM to the joint acceleration space may be different. Comparing the two examples in Fig. 4, it is obvious that in the top configuration, although the green area is smaller, the blue and red areas are larger compared to the bottom plot. It means that, the same CoM accelerations can be achieved by generating smaller accelerations at the joints in the top configuration comparing with the bottom one. This can be explained by CoM dynamic manipulability ellipses as the blue and red ellipses are much more aligned with the green one in the top plot rather than in the bottom one. Note that, blue and red ellipses have the exact same alignments and the only difference is in their sizes. Therefore, in order to minimize the norm of the joint accelerations to reach a certain CoM acceleration, one can minimize the difference in the alignments of these two ellipses.

Since the proposed metric in this paper studies the motion of the CoM, which is the main focus in balancing motions of robots, it can be used to evaluate a robot's ability to balance. Thus, we define *physical ability to balance* as a robot's physical ability to manipulate its CoM in the horizontal directions. Therefore, if we project dynamic manipulability ellipsoids of a robot, in different configurations, onto the horizontal plane, the configuration with the largest ellipse (i.e. projected ellipsoid) will have the highest ability to balance in the sense of the required torque if we use (17) or the required joint accelerations if we use (19) . Note that, the largest projected ellipse is not necessarily the projection from the largest ellipsoid, since the largest ellipsoid might be extended in another (i.e. the vertical) direction. Therefore, by using the CoM dynamic manipulability one can compare different configurations of a robot] or even different robots in terms of their physical abilities to maintain balance.

IV. Conclusion

CoM dynamic manipulability, for legged robots with multiple contacts with the environment, is introduced in this paper in order to study, analyse and measure physical abilities of robots to accelerate their CoMs. Since the proposed metric concerns the motion of the CoM, it is claimed to be a proper tool to study balancing motion and robots' abilities to maintain balance. As a result of the CoM dynamic manipulability analyses in this paper, an ellipsoid in the CoM acceleration space is defined which graphically shows achievable points due to the unit weighted norm of torques at the actuated joints. Two physically meaningful choices for the weights are introduced and discussed in this paper and illustrated by examples. By employing those two choices, CoM manipulability ellipsoids will provide reasonable approximations to the feasible areas of the CoM accelerations due to torque limits and limited joint accelerations.

ACKNOWLEDGMENT

The work presented in this paper is supported by the European Community Framework Programme 7 through the CoDyCo project, contract no. 600716 and also Horizon 2020 through the CogIMon project, contract no. 644727.

REFERENCES

[1] R. Boulic, R. Mas and D. Thalmann. Inverse kinetics for center of mass position control and posture optimization, Proc. Europ. Workshop on Combined Real and Synthetic Image Processing for Broadcast and Video Production, 1994.

[2] A. Bowling and O. Khatib. The dynamic capability equations: a new tool for analyzing robotic manipulator performance. IEEE Trans. Robotics, 21(1):115–123, Feb 2005.

[3] S. Cotton, P. Fraisse and A. Murray. On the manipulability of the center of mass of humanoid robots, application to design. ASME Int. Design Engineering Technical Conf. & Computers and Information in Engineering Conf., pp.1259–1267, Montreal, Canada, Aug 2010.

[4] K. Doty, C. Melchiorri and C. Bonivento. A theory of generalized inverses applied to robotics, Int. J. Robotics Research, 12(1):1–19, Feb 1993.

[5] K. Doty, C. Melchiorri, E. Schwartz and C. Bonivento. Robot manipulability, IEEE Trans. Robotics and Automation, 11(3):462–468, June 1995.

[6] R. Featherstone. Quantitative measures of a robot's ability to balance. Int. Conf. Robotics Science & Systems. Rome, Italy 2015.

[7] A. Goswami. Foot rotation indicator (FRI) point: a new gait planning tool to evaluate postural stability of biped robots. IEEE Int. Conf. Robotics and Automation, pp.47-52, 1999.

[8] A. Goswami and V. Kallem. Rate of change of angular momentum and balance maintenance of biped robots. IEEE Int. Conf. Robotics and Automation. pp. 3785–3790, New Orleans, LA 2004.

[9] Y. Gu, C. Lee and B. Yao. Feasible center of mass dynamic manipulability of humanoid robots. IEEE Int. Conf. Robotics and Automation, pp.5082–5087, Seattle, Washington, May 2015.

[10] L. Guilamo, J. Kuffner, K. Nishiwaki and S. Kagami. Manipulability optimization for trajectory generation. IEEE Int. Conf. Robotics and Automation, pp.2017–2022, Orlando, Florida, May 2006.

[11] T. Hirano, T. Sueyoshi and A. Kawamura. Development of ROCOS(Robot Control Simulator) - jump of human-type biped root by the adaptive impedance control, Proc. 6th Int. Workshop on Advanced Motion Control, 2000.

[12] S. Kagami, F. Kanehiro, Y. Tamiya, M. Inaba and H. Inoue. Autobalancer: an online dynamic balance compensation scheme for humanoid robots, Algorithmic and Computational Robotics: New Directions: the Fourth Workshop on the Algorithmic Foundations of Robotics, pp.329–339, 2001.

[13] S. Kajita, F. Kanehiro, K. Kaneko, K. Fujiwara, K. Harada, K. Yokoi and H. Hirukawa, Resolved momentum control: humanoid motion planning based on the linear and angular momentum, IEEE/RSJ Int. Conf. Intelligent Robots and Systems, pp.1644–1650, Las Vegas, Nevada, Oct 2003.

[14] N. Naksuk and C. Lee. Zero moment point manipulability ellipsoid. IEEE Int. Conf. Robotics and Automation, pp.1970–1975, Orlando, Florida, May 2006.

[15] D. Orin, A. Goswami and S. Lee. Centroidal dynamics of a humanoid robot. Autonomous Robots, 35(2):161–176, October 2013.

[16] D. Prattichizzo, M. Malvezzi, M. Gabiccini and A. Bicchi. On the manipulability ellipsoids of underactuated robotic hands with compliance. Robotics and Autonomous Systems, 60(3):337–346, March 2012.

[17] T. Sugihara. Mobility enhancement control of humanoid robot based on reaction force manipulation via whole body motion. Ph.D. Dissertation, The University of Tokyo, 2003.

[18] T. Sugihara and Y. Nakamura. Whole-body cooperative balancing of humanoid robot using COG Jacobian. IEEE/RSJ Int. Conf. Intelligent Robots and Systems, pp.2575–2580 , Switzerland, Oct 2002.

[19] M. Vukobratović and B. Borovac. Zero-moment point – thirty five years of its life. Int. J. Humanoid Robotics, 1(1):157–173, 2004.

[20] M. Vukobratović, A. Frank and D. Juričić. On the stability of biped locomotion. IEEE Trans. Biomedical Engineering, 17(1):25–26, 1970.

[21] T. Yoshikawa. Manipulability of robotic mechanisms. Int. J. Robotic Research, 4(2):3–9. June 1985.

[22] T. Yoshikawa. Dynamic manipulability of robot manipulators. J. Robot Systems, 2(1):113–124, 1985.